THE JOURNAL OF PHYSICAL CHEMISTRY C

Article

pubs.acs.org/JPCC

Adsorption of Gold and Silver Nanoparticles on Polyelectrolyte Layers and Growth of Polyelectrolyte Multilayers: An In Situ ATR-IR Study

Harekrishna Ghosh and Thomas Bürgi*

Département de Chimie Physique, Université de Genève, Quai Ernest-Ansermet 30, CH-1211 Genève 4, Switzerland

Supporting Information

ABSTRACT: Attenuated total reflection infrared (ATR-IR) spectroscopy is used to study the adsorption of gold and silver nanoparticles and the layer-by-layer (LBL) growth of polyelectrolyte multilayers on a Ge ATR crystal. The Ge ATR crystal is first functionalized using positively charged polyelectrolyte poly(allylamine hydrochloride) (PAH). Then citrate-stabilized gold or silver nanoparticles are adsorbed onto the modified Ge ATR crystal. When gold or silver nanoparticles are adsorbed, a drastic increase of the water signal is observed which is attributed to an enhanced absorption of IR radiation near the nanoparticles. This enhancement was much larger for the silver nanoparticles (SNP). On top of the nanoparticles multilayers of oppositely charged polyelectrolytes PAH and poly(sodium 4-styrenesulfonate) (PSS) were deposited, which allowed to study the enhancement of the IR signals as a function of the distance from the nanoparticles. Furthermore, adsorption of a thiol, *N*-acetyl-L-cysteine, on the nanoparticles confirmed the enhancement. In the case of SNP an absorbance signal of about 15% was observed, which is a factor of about 40 times larger compared to typical signals measure without nanoparticles.

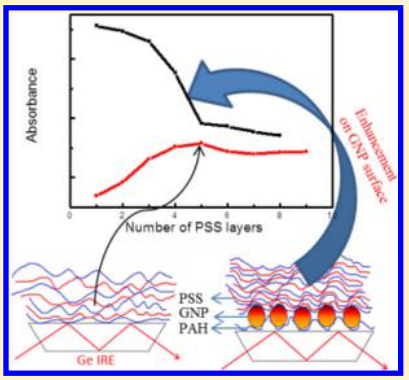

INTRODUCTION

The layer-by-layer (LbL) deposition of polyelectrolytes is a versatile technique to build up multilayers on flat and curved surfaces.[1] The interest in this technique has rapidly grown since its discovery because the preparation of such multilayers is quick, versatile, reliable, and cheap. It is possible to implement the technique on an industrial scale either using a dipping process or by simply spraying the respective solutions onto the substrate.[2] Furthermore, the environmentally friendly, aqueous-solution-based method can be applied to substrates of almost every shape including planar surfaces, colloidal nanoparticles,[3] quantum dots,[3] and porous solids.[4] The technique has found applications in important fields such as biomedicine,[5] solar cells,[6,7] drug delivery,[8] and light-emitting diodes.[9] The LbL technique is not limited to polyelectrolytes. For example, charged particles can be incorporated into polyelectrolyte multilayer systems, thus enlarging the field of application. Hybrid films containing both organic and inorganic materials are of special interest due to their particular electronic and optical properties.[10] For example, charged semiconductor particles[11] or monolayer-protected gold nanoparticles[12] can be incorporated into polyelectrolyte multilayer films.

We recently reported the preparation and optical properties of polyelectrolyte−metal nanoparticle composite films grown on glass slides.[13,14] The citrate-stabilized gold and silver nanoparticles were assembled in layers, and the polyelectrolyte LbL technique allowed one to tune the distance between particles within different layers with nanometer precision. In this way the coupling between the plasmons could be tuned by simply varying the number of polyelectrolyte layers between the nanoparticle arrays. The technique is again not limited to flat surfaces. By using the LbL technique, gold nanoparticles were also assembled around silica beads, which lead to the emergence of a magnetic resonance.[15] Such systems are appealing in the metamaterials field and for the development of cloaking devices.[16]

In the vicinity of the plasmonic particles the electric field can be enhanced. This is used for surface-enhanced Raman scattering (SERS),[17] but even in the infrared enhancement can be observed, leading to surface-enhanced infrared absorption (SEIRA).[18−21] SEIRA has been used to study chemical reactions on metal surfaces,[22] and in general SEIRA is attractive for sensing applications. In contrast to techniques that rely on mass uptake or the change in refractive index, SEIRA yields detailed chemical information since an IR spectrum is a characteristic property of a molecule. Using the finite element method (FEM), it was shown that SEIRA increases with increasing particle size.[23]

In the present study we used attenuated total reflection infrared (ATR-IR) spectroscopy[24−27] to investigate the self-assembly of polyelectrolyte layers and polyelectrolyte−nanoparticle composites. In ATR-IR spectroscopy an evanescent field probes the volume close to the internal reflection element. The penetration depth of the field is several hundred nanometers, which is considerably larger than the typical thickness of polyelectrolyte multilayers (tens of nanometers).

Received: September 16, 2013
Revised: November 29, 2013
Published: December 4, 2013

ATR-IR was used before to study LbL assembly of polyelectrolytes.[28−34] Using ATR-IR, we could follow the LbL assembly of polyelectrolytes and the adsorption of gold and silver nanoparticles on polyelectrolyte films. The infrared absorption was enhanced in the presence of the particles, and the enhancement was about 1 order of magnitude larger for the silver nanoparticles. The LbL technique furthermore allowed us to study the enhancement as a function of the distance from the nanoparticle surface. Because of the enhancement, the adsorption of thiols on the metal particles could be followed easily.

EXPERIMENTAL SECTION

Methods and Materials. Hydrogen tetrachloroaurate(III) hydrate (Alfa Aesar, 99.999% metal basis), silver nitrate (Sigma-Aldrich, 99.9999% metal basis), sodium citrate (Sigma-Aldrich), poly(allylamine hydrochloride) (PAH, Alfa Aesar, average molecular weight of 120 000−200 000), poly(sodium 4-styrenesulfonate) (PSS, Sigma-Aldrich, average molecular weight of 70 000), and *N*-acetyl-L-cysteine (NAC) (Alfa Aesar, 98+%) were used as received. All solutions were prepared using Milli-Q water (18.2 MΩ·cm).

Gold Nanoparticles Solution Preparation. Gold nanoparticles (GNP) solution was prepared according to the well-known Turkevich method.[35−37] In order to prepare spherical GNP with a diameter of about 20 nm in diameter, first 600 mL of a 0.25 mM solution of $HAuCl_4$ under constant magnetic stirring was heated to 100 °C in an oil bath. Then 15 mL of a 0.03 M sodium citrate solution was added to the $HAuCl_4$ solution to reduce the gold ions. A series of color changes were observed up to 20 min. Finally, when the solution changed to a deep-red color, the reaction vessel was removed from the oil bath and allowed to cool to room temperature.

Silver Nanoparticles Solution Preparation. Silver nanoparticles (SNP, ∼6 nm in diameter) were prepared in the following way.[38] In a 500 mL round bottle flask, 196 mL of Milli-Q water was cooled down to 10 °C. Then 2 mL of aqueous solutions of $AgNO_3$ (25 mM) and sodium citrate (25 mM) were added under vigorous magnetic stirring. Then 600 μL of an aqueous ice-cooled $NaBH_4$ (0.1 M) solution was added to that solution in a dropwise fashion. After 2 h the mixture was yellow, indicating completion of the reaction. The solution was kept in the fridge until used. Both SNP and GNP show characteristic plasmon bands in their UV−vis spectra (see Supporting Information S1).

Preparation of Polyelectrolyte and *N*-Acetyl-L-cysteine (NAC) Solution. 1 mg/mL of PAH and PSS were dissolved in a 0.1 M solution of sodium chloride in water to prepare solutions of positive and negative polyelectrolyte, respectively. Solutions of NAC were prepared at a concentration of 4 mM in water.

Instruments. Scanning electron microscopy (SEM, JEOL JSM-7600F) was used to characterize the attached GNP on the surface of a functionalized Ge internal reflection element used for ATR spectroscopy. UV−vis spectra were recorded on a Cary Varian 50 Bio UV−vis spectrometer. Transmission electron microscopy (TEM) was performed using a TEM-Tecnai G2.

Functionalization of Ge Elements for ATR-IR Spectroscopy. Ge internal reflection elements (IREs; 50 mm × 20 mm × 1 mm, Komlas) were used for ATR-IR experiments. The IREs were first polished with a 0.25 μm grain size diamond paste (Buehler, Metadi II) and afterward rinsed copiously with Milli-Q water before the surface was plasma cleaned under a flow of air for 2 min (Harrick Plasma Instrument). Then the plasma cleaned Ge ATR crystal was functionalized by adsorption of the positively charged polyelectrolyte PAH. That functionalized Ge surface is used for gold and silver nanoparticle adsorption and for further studies.

ATR-IR Measurements. ATR-IR spectra were measured with a Bruker VERTEX 80v Fourier transform infrared (FT-IR) spectrometer with a liquid nitrogen cooled narrow-band mercury cadmium telluride (MCT) detector. Spectra were recorded at a resolution of 4 cm^{-1}. For in situ ATR-IR experiments a dedicated flow-through cell was used made from a Teflon piece and a fused silica plate (64 mm × 30 mm × 5 mm) with holes for inlet and outlet (39 mm apart) and a Viton seal (1 mm). The volume of the used flow-through cell is 0.129 mL with a gap of 270 μm.[39] The cell was mounted on an attachment for ATR measurements within the sample compartment of the FTIR spectrometer. The solutions were passed through the cell and over the Ge crystal at a flow rate of 0.5 mL/min by means of a peristaltic pump (Ismatec, Reglo 100) located in front of the cell. The angle of incidence was 45°, and only one side of the Ge IRE was used leading to 20 active reflections. All experiments were performed at room temperature, and the spectrometer was evacuated to avoid contributions from gas-phase water and CO_2.

RESULTS AND DISCUSSION

Polyelectrolyte Adsorption on Ge IRE. During plasma treatment a thin oxide layer is formed on the surface of the Ge IRE. The positive polyelectrolyte PAH adsorbs spontaneously on this surface, whereas negatively charged PSS does not. Adsorption can be followed in situ by ATR-IR. Figure 1 shows

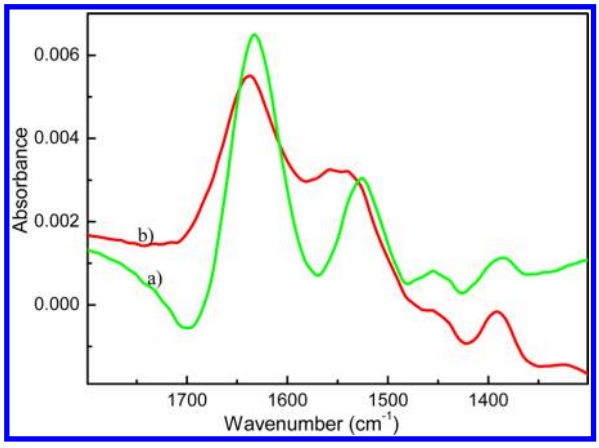

Figure 1. ATR-IR spectra recorded during adsorption of PAH and subsequent washing. (a) Polyelectrolyte adsorption from 0.1 M NaCl solution; (b) washing for 90 min with neat water. For both spectra the reference was recorded while flowing neat water before the adsorption step.

ATR-IR spectra of the positive electrolyte PAH after adsorption from 0.1 M NaCl solution and after washing with neat water. Note that the reference for both spectra was recorded before the adsorption of the polyelectrolyte while flowing neat water over the Ge IRE. The initial adsorption of the polyelectrolyte is very fast, and it reaches saturation within 10 min. The most prominent bands in the spectrum of adsorbed PAH (Figure 1a) at 1630 and 1530 cm^{-1} are assigned to the asymmetric and symmetric bending vibration of the protonated amine groups

dx.doi.org/10.1021/jp409241t | J. Phys. Chem. C 2013, 117, 26652−26658

$[NH_3]^+$, respectively.[40,41] The negative band at 1700 cm^{-1} is due to dissolved NaCl, which influences the water spectrum. This band arises because in spectrum a in Figure 1 the adsorption of the polyelectrolyte was performed in NaCl solution, whereas the reference was taken in neat water. Upon flowing neat water over the sample (spectrum b in Figure 1), this negative band disappears and the band at 1530 cm^{-1} shifted to 1560 cm^{-1} (Figure 1).[42] This is explained by a partial deprotonation of the $[NH_3]^+$ groups due to a slight pH change upon changing from polyelectrolyte solution to neat water. Most importantly, Figure 1 shows that the adsorption of the positively charged polyelectrolyte on Ge is successful. Such as surface is now prepared for the adsorption of negatively charged nanoparticles.

Adsorption of Nanoparticles on Functionalized Ge IRE. Figure 2 shows ATR-IR spectra recorded in situ during the adsorption of GNP on the functionalized Ge surface. Several peaks are observed in the spectrum at 3400, 1570, 1390, and 1640 cm^{-1}, which are due to the water stretching modes, the asymmetric and symmetric carboxylate stretching modes of citrate, and the water bending mode, respectively. The nanoparticle solution contains citrates, both free and adsorbed on the nanoparticles. The initially very fast adsorption of citrate (peaks at 1570 and 1390 cm^{-1}) is due to adsorption of dissolved citrate on positively charged PE. This was proved by repeating the same experiment using dialyzed GNP solution (see Supporting Information S2). In this case almost all free citrate ligands were removed by dialysis.

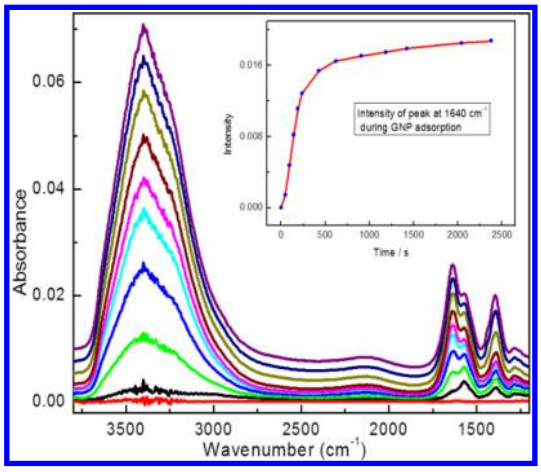

Figure 2. ATR-IR spectra of GNP adsorption on a PAH functionalized Ge IRE. Spectra were measured during the adsorption of GNP, and the background spectrum was taken just before GNP adsorption. After taking the background (red spectrum), the first five spectra were measured in time intervals of 48 s. The last spectrum was measured after 40 min.

During the adsorption of GNP the absorbance of the water peaks is increasing. Usually negative solvent peaks are observed in the ATR-IR spectra upon adsorption of (large) molecules at the solid–liquid interface due to the displacement of solvent because with respect to the reference measurement less solvent molecules are probed by the evanescent field. Here the opposite effect is observed, i.e. an increase of the water peaks. This effect is explained by an enhanced infrared absorption near the GNP, which overcompensates the loss of water molecules within the evanescent field due to adsorption of the nanoparticles. GNPs do not have fundamental vibrational modes in the spectral region shown in Figure 2. However, the water absorption allows one to follow indirectly the adsorption of the GNP. Initially adsorption was very fast, and then slowly it reached saturation after around 40 min (see inset in Figure 2).

Initially the absorbance of the citrate peaks was larger than the one of the water peaks. This can be explained by the fast adsorption of unbound (dissolved) citrates on the positively charged PE surface followed by the slower adsorption of citrate capped GNP. When applying a washing step, the spectrum did not change, which shows that the adsorbed GNPs are stable on the Ge surface. However, the absorbance of citrate peaks at 1570 and 1390 cm^{-1} are very sensitive to the nature of the solution and pH. When adsorbed GNP was washed with Milli-Q water, the absorbance of the citrate peaks did not change. However, when 0.1 M NaCl solution was flowed over the stable GNP surface, the absorbance of the citrate peaks decreased (Figure 3). Similar behavior was observed when a solution of positive electrolyte PAH in 0.1 M NaCl was flowed over the adsorbed GNPs (Supporting Information S3). This shows that in the presence of NaCl citrate is removed from the surface. The citrate is replaced by water, which leads to the positive band in the spectrum at about 1640 cm^{-1}.

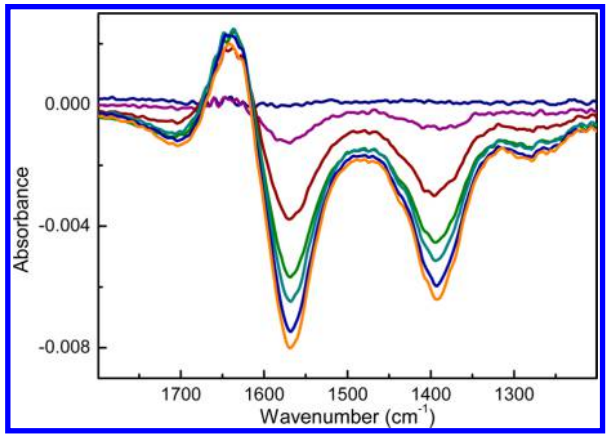

Figure 3. ATR-IR spectra of citrate-stabilized GNPs adsorbed on PAH-functionalized Ge IRE during the flow of 0.1 M NaCl solution. The background was taken after GNP adsorption and a neat water washing step, just before flowing the NaCl solution. The negative peaks indicate removal of citrate from the surface upon flowing NaCl solution.

Analogous experiments to the ones described above were repeated with silver instead of gold nanoparticles. A comparison of the corresponding ATR-IR spectra after adsorption is shown in Figure 4. The IR bands are much stronger in the case of silver nanoparticles (SNP). For example, the band associated with the water bending mode is about 9 times stronger for SNP than for GNP. For the citrate bands the enhancement is even stronger. For example, the symmetric carboxylate stretching mode of citrate is stronger by a factor of over 13 in the SNP case. It is difficult to quantify the intrinsic enhancement for the two cases because other factors enter into play such as the different effective surface area for the two samples (different coverage and interparticle separation and different size of the particles). Larger particles should give stronger enhancement.[23] As the smaller silver nanoparticles give stronger enhancement than the larger gold nanoparticles, we conclude that other factors than particle size play a dominant role in our case. It is

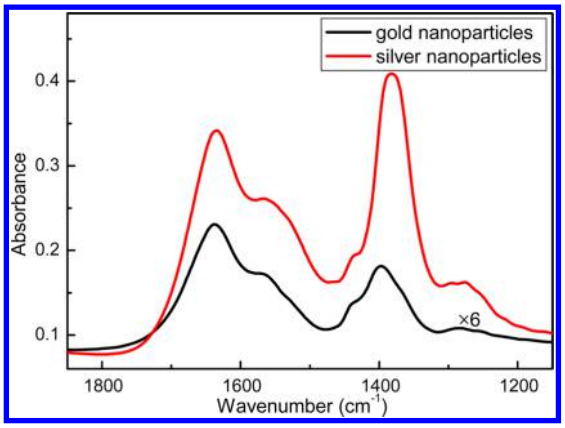

Figure 4. ATR-IR spectra of adsorbed GNP and SNP on PAH-modified Ge surface. In both cases the background was taken before particles adsorption. GNP was adsorbed up to 40 min, whereas SNP was adsorbed up to 70 min to reach saturation. The GNP spectrum was scaled by a factor of 6.

interesting to note that the relative enhancement in the silver case is larger for adsorbed citrate than for (bulk) water.

SEM Images of GNP on Functionalized Ge Surface. Figure 5 shows the SEM images of GNPs adsorbed on a

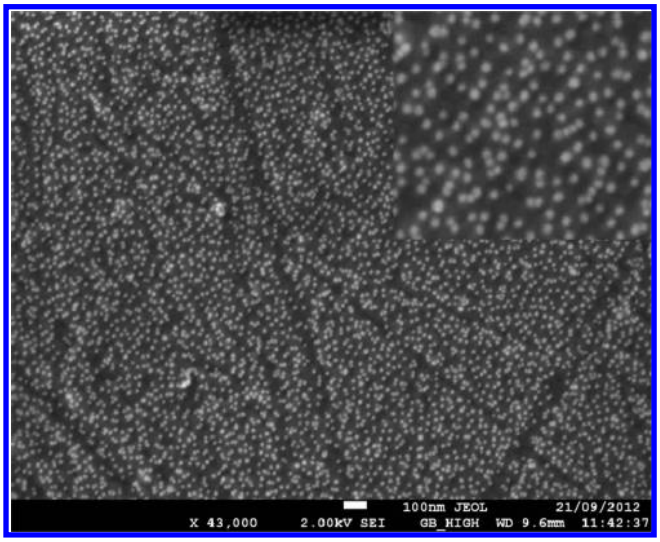

Figure 5. SEM Images of GNP on a functionalized Ge surface. The Ge ATR crystal was plasma cleaned before PAH functionalization. After 40 min of GNP adsorption the crystal surface was washed with copious amounts of neat water.

functionalized Ge ATR crystal surface. The spherical GNP of around 20 nm in diameter are well dispersed. This is due to the mutual repulsion between adsorbed nanoparticles as a consequence of Coulomb interaction. The particle density on the surface is 650 particles/μm^2, which corresponds to a coverage of about 20%. Because of the small size of the SNP (around 6 nm in diameter, see TEM image in the Supporting Information S7), SEM did not yield useful information in this case.

Layer-by-Layer Deposition of Polyelectrolytes. We further studied the layer-by-layer deposition of positively and negatively charged PE on the blank Ge surface. The positive charge of the amine group on the functionalized Ge surface allows the attachment of GNP as well as negatively charged polyelectrolyte through electrostatic interactions. The strong IR peaks of PSS allow one to follow the growth of the multilayers.

Figure 6 shows ATR-IR spectra of an experiment where a polyelectrolyte multilayer was grown on the Ge IRE by

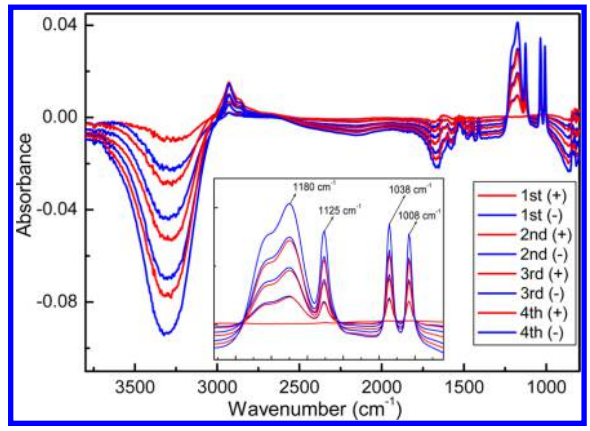

Figure 6. In situ ATR-IR spectra recorded during layer by layer growth of positively and negatively charged PE on a Ge ATR crystal surface. The background was taken in 0.1 M NaCl solution before the PAH/PSS LBL attachment was done. Washing was done in between each PE layer attachment step with NaCl solution. Spectra were recorded at the end of each washing step. The time needed for each adsorption and washing step was about 10 min.

alternatively flowing positively and negatively charged PE over the sample. Characteristic peaks of negatively charged PSS are assigned as follows: The peak at 1180 cm^{-1} is due to the asymmetric stretching vibration of SO_3, the peak at 1125 cm^{-1} is due to an aromatic ring vibration, the one 1038 cm^{-1} is due to the SO_3 symmetric stretching vibration, and the band at 1008 cm^{-1} is due to a C−H bending mode of the aromatic ring.[43] Figure 6 reveals negative water peaks at 3300 and 1665 cm^{-1}, which arise due to the displacement of water from the volume probed by the evanescent field upon polyelectrolyte adsorption. It is clear from the spectra that the amount of water displaced is more important for the negative polyelectrolyte. A quantitative analysis reveals that the change of the water absorbance at 3300 cm^{-1} is larger for PSS than for PAH by a factor of 1.85 for first bilayer, 2 for second bilayer, 2.25 for third bilayer, and 2.5 for fourth bilayer. The observation that PSS displaces more water than PAH can be explained in the following way: The adsorption of a polyelectrolyte on a layer of oppositely charged polyelectrolyte is charge-driven. The number of charges in each layer should therefore be about the same. However, the unit volume per unit charge is not the same for the two polyelectrolytes. A rough estimate (see Supporting Information) gives a relative value of 3.1 for the two polyelectrolytes used in this study; i.e., the negative polyelectrolyte uses about 3.1 times more volume than the positively charged polyelectrolyte. This value is close the one determined from the ATR-IR experiment, particularly in the upper layers.

Nanoparticle PE Multilayer Composites. The growth of successive polyelectrolyte layer on blank Ge as well as on top of a GNP layer was quantitatively followed by in situ ATR-IR spectroscopy. For this the change of absorbance of the most prominent peak of PSS at 1176 cm^{-1} was measured after deposition of each (PAH/PSS) layer. Figure 7 shows the result for $(PAH/PSS)_n$ (n = 1−9) and (PAH/GNP)$(PAH/PSS)_n$ (n = 1−8). For the system without GNP the increase of the PSS

dx.doi.org/10.1021/jp409241t | J. Phys. Chem. C 2013, 117, 26652−26658

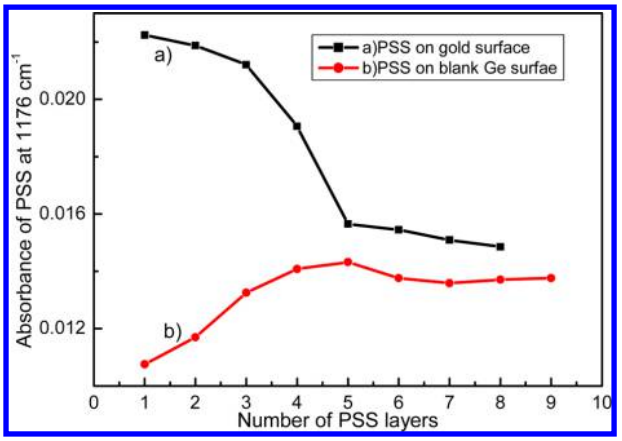

Figure 7. Increase of absorbance of the PSS peak at 1176 cm^{-1} in the ATR-IR spectra as a function of adsorbed PSS layers (a) with GNP (PAH/GNP)$(PAH/PSS)_n$ (n = 1−8) and (b) without GNP $(PAH/PSS)_n$ (n = 1−9).

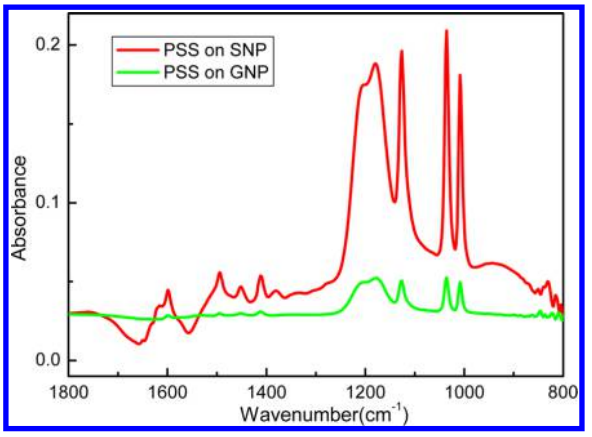

Figure 8. ATR-IR spectra of PSS on GNP and SNP surfaces. The background was taken before PSS adsorption. After adsorption of particles and washing with neat water, PAH solution was flowed over the sample to make the surface positively charged, and then PSS adsorption was performed.

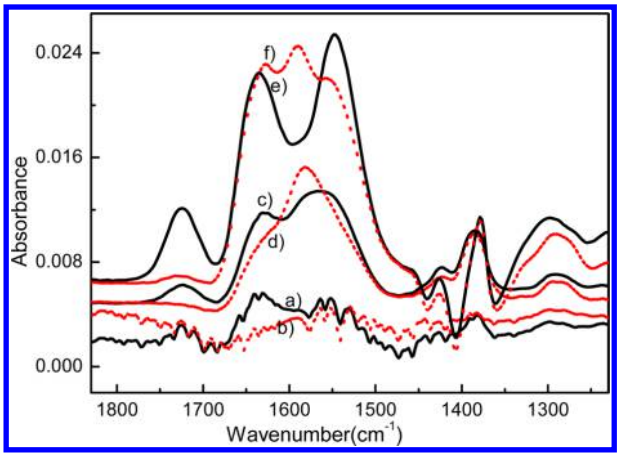

Figure 9. ATR-IR spectra of NAC adsorption and washing: (a) adsorption and (b) washing on blank Ge surface; (c) adsorption and (d) washing on PAH surface; (e) adsorption and (f) washing on GNP surface. In all three cases the background was taken before adsorption of NAC on the respective surfaces, and then adsorption was continued up to saturation. Washing was done with neat water.

absorbance value per layer slightly increases from about 0.0107 for the first layer to about 0.0143 absorbance units for the fifth layer, which corresponds to an increase by 34%, and stays more or less constant afterward. This indicates that in the very first layers less PSS is adsorbed and that after 5 layers the adsorbed amount per step stays constant. Note that supralinear film growth has been observed before.[44] The behavior is completely different for the system with the GNP. Here the absorbance of the PSS peak is strongest for the first layer and then decreases until reaching an almost constant value after five depositions. Note that the absorbance of the first deposition is about double compared to the system without GNP, whereas after five depositions the absorbance increases are similar. Both the stronger absorbance as compared to the system without the GNP and the decrease of the absorbance for successive layers can be explained by the enhancement of the IR absorption due to the GNP. The electric field enhancement is expected to decay from the nanoparticle surface, and the layer-by-layer experiment can actually "measure" this decay. From Figure 7 it can be seen that enhancement is observed up to 4−5 layers. One PE double layer has a thickness of about 2.5 nm.[45,46] Therefore, we can conclude that the enhancement can be observed in this case up to a distance of 10−12 nm from the nanoparticle surface, which corresponds to about one nanoparticle radius. As expected, the largest enhancement is observed for the very first layer, which is closest to the nanoparticles surface. However, the absorbance from the second PSS layer is almost as large.

Figure 8 shows the ATR-IR spectra of one PSS layer on the top of GNPs and SNPs, respectively. The particles were first adsorbed on the functionalized Ge IRE crystal surface, and then PAH solution (1 mg PAH/mL in 0.1 M NaCl) was flowed over the sample to make the particles surface positively charged. After washing with neat water, the background was measured before the adsorption of PSS (1 mg/mL PSS in 0.1 M NaCl) and measurement of the ATR-IR spectra. The absorbance of PSS on SNP is more than 8 times stronger compared to the GNP case, in line with the enhancement observed for the water and citrate bands due to GNPs and SNPs (Figure 4).

Adsorption of a Thiol on GNPs and SNPs. Figure 9 shows ATR-IR spectra measured during adsorption of NAC on different surfaces and after washing with neat water. First we tried to adsorb NAC from aqueous solution directly on a plasma cleaned blank Ge IRE surface (spectrum a in Figure 9). Only very small bands could be observed due to adsorbed NAC, and during rinsing with water (spectrum b in Figure 9) the NAC desorbed. The behavior was different when the plasma cleaned Ge IRE was first functionalized with PAH. In this case NAC adsorption was evident (spectrum c in Figure 9) with its characteristic peaks at 1721, 1631, 1561, and 1385 cm^{-1} due to the carboxylic acid stretching, amide I vibration, amide II vibration, and symmetric carboxylate stretching, respectively. During neat water washing spectral changes were observed, which we ascribe to the change of pH (pH 3 for NAC solution and pH 5.8 for water). Notably the carboxylic acid stretching peak at 1721 cm^{-1} disappeared whereas the asymmetric carboxylate stretching peak appeared at 1584 cm^{-1} [47] (spectrum d in Figure 9). Finally NAC was adsorbed on the GNP attached to PAH functionalized Ge (spectrum e in Figure 9). The thiol has a high affinity for gold. As is evident from Figure 9, the NAC bands are even stronger in this case, which we again ascribe to the enhancement effect due to gold. In addition, the spectrum also changed qualitatively, which

dx.doi.org/10.1021/jp409241t | J. Phys. Chem. C 2013, 117, 26652−26658

indicates a different interaction of NAC with gold than with PAH. Note that in the experiment with the GNP some NAC is probably also adsorbing on the free PAH surface.

The adsorption of NAC was repeated on the SNPs. The spectrum is compared to the one recorded for GNP in Figure 10. The spectra look qualitatively the same but different from the spectrum recorded for NAC on PAH (Figure 9). However, the bands of NAC on silver are stronger by a factor of about 9, which we ascribe again to the stronger enhancement on SNPs than on GNPs.

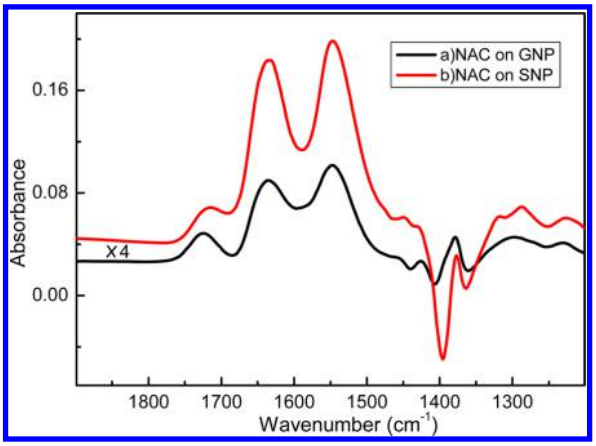

Figure 10. ATR-IR spectra of NAC adsorption on nanoparticles: (a) adsorption of NAC on GNP surface and (b) adsorption of NAC on SNP surface. The background was taken before adsorption of NAC on the respective particle surfaces, and then adsorption was continued up to saturation. The NAC ATR-IR spectrum on GNP surface was scaled a factor of 4.

CONCLUSIONS

ATR-IR spectroscopy is a valuable tool to study polyelectrolyte−nanoparticle composite films. Upon adsorption of polyelectrolyte, negative bands of displaced water can be observed besides the bands of the polyelectrolyte. The adsorption of gold and silver nanoparticles is evidenced by the water bands. These bands are positive, despite the displacement of water, due to enhanced infrared absorption near the nanoparticles. Citrate ions that stabilize the nanoparticles can also be evidenced. Enhanced infrared absorption was also found for thiols adsorbed on the nanoparticles and for polyelectrolyte multilayers built on top of the nanoparticles. The latter system allows one to study the enhancement as a function of the distance from the nanoparticles surface. For gold nanoparticles with 20 nm diameter the enhancement was observed up to a distance of about 10 nm from the nanoparticle surface, that is, up to about one nanoparticle radius. The enhancement observed for silver nanoparticle layers was almost 1 order of magnitude larger than the one for gold nanoparticles.

ASSOCIATED CONTENT

Supporting Information

UV−vis spectra of GNP and SNP in water, ATR-IR spectra of dialyzed GNP, ATR-IR spectra of GNP attached to a Ge IRE surface during the flow of PAH solution, ATR-IR spectra of PAH and PSS on blank Ge and GNP surface, volume calculation of polyelectrolyte bilayer, ATR-IR spectra of NAC on blank Ge and SNP surface and TEM image of SNP. This material is available free of charge via the Internet at http://pubs.acs.org.

AUTHOR INFORMATION

Corresponding Author

*E-mail Thomas.buergi@unige.ch; tel ++41 (0)22 379 65 52 (T.B.).

Notes

The authors declare no competing financial interest.

ACKNOWLEDGMENTS

The work was supported by the Swiss National Science Foundation and the University of Geneva.

ABBREVIATIONS

ATR-IR, attenuated total reflection infrared; PAH, poly(allylamine hydrochloride); PSS, poly(sodium 4-styrenesulfonate); GNP, gold nanoparticle; SNP, silver nanoparticle; PE, polyelectrolyte.

REFERENCES

(1) Decher, G. Fuzzy Nanoassemblies: Toward Layered Polymeric Multicomposites. *Science* **1997**, *277*, 1232−1237.

(2) Izquierdo, A.; Ono, S. S.; Voegel, J. C.; Schaaf, P.; Decher, G. Dipping Versus Spraying: Exploring the Deposition Conditions for Speeding up Layer-by-Layer Assembly. *Langmuir* **2005**, *21*, 7558−7567.

(3) Sukhorukov, G. B.; Donath, E.; Lichtenfeld, H.; Knippel, E.; Knippel, M.; Budde, A.; Möhwald, H. Layer-by-Layer Self Assembly of Polyelectrolytes on Colloidal Particles. *Colloids Surf., A* **1998**, *137*, 253−266.

(4) Sukhorukov, G. B.; Volodkin, D. V.; Gunther, A. M.; Petrov, A. I.; Shenoy, D. B.; Mohwald, H. Porous Calcium Carbonate Microparticles as Templates for Encapsulation of Bioactive Compounds. *J. Mater. Chem.* **2004**, *14*, 2073−2081.

(5) Tang, Z. Y.; Wang, Y.; Podsiadlo, P.; Kotov, N. A. Biomedical Applications of Layer-by-Layer Assembly: From Biomimetics to Tissue Engineering. *Adv. Mater.* **2006**, *18*, 3203−3224.

(6) He, J. A.; Mosurkal, R.; Samuelson, L. A.; Li, L.; Kumar, J. Dye-Sensitized Solar Cell Fabricated by Electrostatic Layer-by-Layer Assembly of Amphoteric TiO_2 Nanoparticles. *Langmuir* **2003**, *19*, 2169−2174.

(7) Agrios, A. G.; Cesar, I.; Comte, P.; Nazeeruddin, M. K.; Gratzel, M. Nanostructured Composite Films for Dye-Sensitized Solar Cells by Electrostatic Layer-by-Layer Deposition. *Chem. Mater.* **2006**, *18*, 5395−5397.

(8) Sukhorukov, G. B.; Rogach, A. L.; Zebli, B.; Liedl, T.; Skirtach, A. G.; Kohler, K.; Antipov, A. A.; Gaponik, N.; Susha, A. S.; Winterhalter, M.; Parak, W. J. Nanoengineered Polymer Capsules: Tools for Detection, Controlled Delivery, and Site-Specific Manipulation. *Small* **2005**, *1*, 194−200.

(9) Eckle, M.; Decher, G. Tuning the Performance of Layer-by-Layer Assembled Organic Light Emitting Diodes by Controlling the Position of Isolating Clay Barrier Sheets. *Nano Lett.* **2001**, *1*, 45−49.

(10) Peng, C. Q.; Thio, Y. S.; Gerhardt, R. A. Conductive Paper Fabricated by Layer-by-Layer Assembly of Polyelectrolytes and Ito Nanoparticles. *Nanotechnology* **2008**, *19*.

(11) Kotov, N. A.; Dekany, I.; Fendler, J. H. Layer-by-Layer Self-Assembly of Polyelectrolyte-Semiconductor Nanoparticle Composite Films. *J. Phys. Chem.* **1995**, *99*, 13065−13069.

(12) Hicks, J. F.; Seok-Shon, Y.; Murray, R. W. Layer-by-Layer Growth of Polymer/Nanoparticle Films Containing Monolayer-Protected Gold Clusters. *Langmuir* **2002**, *18*, 2288−2294.

(13) Cunningham, A.; Muhlig, S.; Rockstuhl, C.; Burgi, T. Coupling of Plasmon Resonances in Tunable Layered Arrays of Gold Nanoparticles. *J. Phys. Chem. C* **2011**, *115*, 8955−8960.

(14) Cunningham, A.; Muhlig, S.; Rockstuhl, C.; Burgi, T. Exciting Bright and Dark Eigenmodes in Strongly Coupled Asymmetric Metallic Nanoparticle Arrays. *J. Phys. Chem. C* **2012**, *116*, 17746−17752.
(15) Muhlig, S.; Cunningham, A.; Scheeler, S.; Pacholski, C.; Burgi, T.; Rockstuhl, C.; Lederer, F. Self-Assembled Plasmonic Core-Shell Clusters with an Isotropic Magnetic Dipole Response in the Visible Range. *ACS Nano* **2011**, *5*, 6586−6592.
(16) Mühlig, S.; Cunningham, A.; Dintinger, J.; Farhat, M.; Hasan, S. B.; Scharf, T.; Bürgi, T.; Lederer, F.; Rockstuhl, C. A Self-Assembled Three-Dimensional Cloak in the Visible. *Sci. Rep.* **2013**, *3*.
(17) Campion, A.; Kambhampati, P. Surface-Enhanced Raman Scattering. *Chem. Soc. Rev.* **1998**, *27*, 241−250.
(18) Osawa, M. Dynamic Processes in Electrochemical Reactions Studied by Surface-Enhanced Infrared Absorption Spectroscopy (Seiras). *Bull. Chem. Soc. Jpn.* **1997**, *70*, 2861−2880.
(19) Enders, D.; Nagao, T.; Pucci, A.; Nakayama, T.; Aono, M. Surface-Enhanced ATR-IR Spectroscopy with Interface-Grown Plasmonic Gold-Island Films near the Percolation Threshold. *Phys. Chem. Chem. Phys.* **2011**, *13*, 4935−4941.
(20) Neubrech, F.; Pucci, A.; Cornelius, T. W.; Karim, S.; Garcia-Etxarri, A.; Aizpurua, J. Resonant Plasmonic and Vibrational Coupling in a Tailored Nanoantenna for Infrared Detection. *Phys. Rev. Lett.* **2008**, *101*.
(21) Osawa, M.; Ataka, K.-I.; Yoshii, K.; Nishikawa, Y. Surface-Enhanced Infrared Spectroscopy: The Origin of the Absorption Enhancement and Band Selection Rule in the Infrared Spectra of Molecules Adsorbed on Fine Metal Particles. *Appl. Spectrosc.* **1993**, *47*, 1497−1502.
(22) Cai, W. B.; Wan, L. J.; Noda, H.; Hibino, Y.; Ataka, K.; Osawa, M. Orientational Phase Transition in a Pyridine Adlayer on Gold(111) in Aqueous Solution Studied by in Situ Infrared Spectroscopy and Scanning Tunneling Microscopy. *Langmuir* **1998**, *14*, 6992−6998.
(23) Vasan, G.; Chen, Y.; Erbe, A. Computation of Surface-Enhanced Infrared Absorption Spectra of Particles at a Surface through the Finite Element Method. *J. Phys. Chem. C* **2011**, *115*, 3025−3033.
(24) Harrick, N. J. Study of Physics and Chemistry of Surfaces from Frustrated Total Internal Reflections. *Phys. Rev. Lett.* **1960**, *4*, 224−226.
(25) Fahrenfort, J. Attenuated Total Reflection - a New Principle for the Production of Useful Infra-Red Reflection Spectra of Organic Compounds. *Spectrochim. Acta* **1961**, *17*, 698.
(26) Ferri, D.; Burgi, T.; Baiker, A. Pt and Pt/Al_2O_3 Thin Films for Investigation of Catalytic Solid-Liquid Interfaces by ATR-IR Spectroscopy: Co Adsorption, H-2-Induced Reconstruction and Surface-Enhanced Absorption. *J. Phys. Chem. B* **2001**, *105*, 3187−3195.
(27) Burgi, T.; Baiker, A.; Gates, B. C.; Knozinger, H. *Adv. Catal.* **2006**, *50*, 227−283.
(28) Zhong, W.; Liu, Z.; Tomasik, P.; Jin, H.; Lv, N.; Meng, S.; Guo, Z.; Wu, L. *e-Polym.* **2008**, *8*, 1605.
(29) Serizawa, T.; Kawanishi, N.; Akashi, M. Layer-by-Layer Assembly between Poly(Vinylamine Hydrochloride-Co-N-Vinylformamide) with Variable Primary Amine Content and Poly(Sodium Styrenesulfonate). *Macromolecules* **2003**, *36*, 1967−1974.
(30) Kharlampieva, E.; Jung, C. M.; Kozlovskaya, V.; Tsukruk, V. V. Secondary Structure of Silaffin at Interfaces and Titania Formation. *J. Mater. Chem.* **2010**, *20*, 5242−5250.
(31) Cho, C.-W.; Lee, S.-M.; Paik, U.; Yoon, S.-M.; Choi, J.-Y.; Lee, H. S. Self-Assembled Single Walled Carbon Nanotubes on Multi-Layered Polyelectrolyte Layer. *Colloids Surf., A* **2008**, *313−314*, 419−421.
(32) Jiang, G.; Baba, A.; Ikarashi, H.; Xu, R.; Locklin, J.; Kashif, K. R.; Shinbo, K.; Kato, K.; Kaneko, F.; Advincula, R. Signal Enhancement and Tuning of Surface Plasmon Resonance in Au Nanoparticle/Polyelectrolyte Ultrathin Films. *J. Phys. Chem. C* **2007**, *111*, 18687−18694.
(33) Zhong, X.; Lu, Z.; Valtchev, P.; Wei, H.; Zreiqat, H.; Dehghani, F. Surface Modification of Poly(Propylene Carbonate) by Aminolysis and Layer-by-Layer Assembly for Enhanced Cytocompatibility. *Colloids Surf., B* **2012**, *93*, 75−84.
(34) Bae, W.-S.; Convertine, A. J.; McCormick, C. L.; Urban, M. W. Effect of Sequential Layer-by-Layer Surface Modifications on the Surface Energy of Plasma-Modified Poly(Dimethylsiloxane). *Langmuir* **2006**, *23*, 667−672.
(35) Turkevich, J.; Stevenson, P. C.; Hillier, J. A Study of the Nucleation and Growth Processes in the Synthesis of Colloidal Gold. *Discuss. Faraday Soc.* **1951**, *11*, 55−75.
(36) Kimling, J.; Maier, M.; Okenve, B.; Kotaidis, V.; Ballot, H.; Plech, A. Turkevich Method for Gold Nanoparticle Synthesis Revisited. *J. Phys. Chem. B* **2006**, *110*, 15700−15707.
(37) Frens, G. Controlled Nucleation for the Regulation of the Particle Size in Monodisperse Gold Suspensions. *Nature (London), Phys. Sci.* **1973**, *241*, 20−22.
(38) Cunningham, A. Ph.D Thesis, Bottom-up Organisation of Metallic Nanoparticles for Metamaterials Applications. University of Geneva, 2012.
(39) Völker, B.; Wölzl, F.; Bürgi, T.; Lingenfelser, D. Dye Bonding to TiO_2: In Situ Attenuated Total Reflection Infrared Spectroscopy Study, Simulations, and Correlation with Dye-Sensitized Solar Cell Characteristics. *Langmuir* **2012**, *28*, 11354−11363.
(40) Jaber, J. A.; Schlenoff, J. B. Counterions and Water in Polyelectrolyte Multilayers: A Tale of Two Polycations. *Langmuir* **2007**, *23*, 896−901.
(41) Camacho, S. A.; Aoki, P. H. B.; Constantino, C. J. L.; Aroca, R. F.; Pires, A. M. Nanostructured Hybrid Films Containing Nanophosphor: Fabrication and Electronic Spectral Properties. *J. Alloys Compd.* **2012**, *541*, 365−371.
(42) Tóháti, H.-M.; Botka, B.; Németh, K.; Pekker, Á.; Hackl, R.; Kamarás, K. Infrared and Raman Investigation of Carbon Nanotube-Polyallylamine Hybrid Systems. *Physica Status Solidi B* **2010**, *247*, 2884−2886.
(43) Kim, J.-H.; Kim, S.-K.; Nam, K.; Kim, D.-W. Composite Proton Conducting Membranes Based on Nafion and Sulfonated SiO_2 Nanoparticles. *J. Membr. Sci.* **2012**, *415−416*, 696−701.
(44) Elbert, D. L.; Herbert, C. B.; Hubbell, J. A. Thin Polymer Layers Formed by Polyelectrolyte Multilayer Techniques on Biological Surfaces. *Langmuir* **1999**, *15*, 5355−5362.
(45) Bosio, V.; Dubreuil, F.; Bogdanovic, G.; Fery, A. Interactions between Silica Surfaces Coated by Polyelectrolyte Multilayers in Aqueous Environment: Comparison between Precursor and Multilayer Regime. *Colloids Surf., A* **2004**, *243*, 147−155.
(46) Caruso, F.; Niikura, K.; Furlong, D. N.; Okahata, Y. 1. Ultrathin Multilayer Polyelectrolyte Films on Gold: Construction and Thickness Determination. *Langmuir* **1997**, *13*, 3422−3426.
(47) Bieri, M.; Bürgi, T. Enantiodiscrimination between an N-Acetyl-L-Cysteine Sam and Proline: An in Situ Spectroscopic and Computational Study. *ChemPhysChem* **2006**, *7*, 514−523.